RSC Advances

ROYAL SOCIETY OF CHEMISTRY

www.rsc.org/advances

Preparation and thermoelectric properties of diphenylaminobenzylidene-substituted poly(3-methylthiophene methine)/graphite composite

Junjie Li,[a] Lei Wang,*[,a] Xiaole Jia,[a] Xiongzhi Xiang,[a] Cheuk-Lam Ho,[b] Wai-Yeung Wong*[,b] and Hua Li[c]

[a] *Shenzhen Key Laboratory of Special Functional Materials, College of Materials Science and Engineering, Shenzhen University, Shenzhen 518060, P.R. China*

E-mail: wl@szu.edu.cn

[b] *Institute of Molecular Functional Materials, Department of Chemistry and Partner State Key Laboratory of Environmental and Biological Analysis, Hong Kong Baptist University, Waterloo Road, Kowloon Tong, Hong Kong, P.R. China*

E-mail: rwywong@hkbu.edu.hk

[c] *College of Life and Environmental Sciences & Beijing Engineering Research Center of Food Environment and Public Health, Minzu University of China, Beijing 100081, P.R. China*

Abstract

Polymer-inorganic composites show great potential for use as thermoelectric (TE) materials. However, the TE performance of these materials needs to be improved. One way to improve the TE performance would be to synthesize novel conductive polymers with high Seebeck coefficients to prepare polymer-inorganic TE composites. In this study, acidized and ammoniated forms of poly[(3-methylthiophene-2,5-diyl)(diphenylaminobenzylidene) (3-methylthiophene quinodimethane-2,5-diyl)] (PMTDPABQ) were successfully synthesized with high Seebeck coefficients. These polymers were used to prepare a series of PMTDPABQ/graphite (G) bulk composites by mechanical ball milling and cold pressing. The morphology, thermal stability, and TE performance of these composites were evaluated. The G composite was uniformly dispersed in the polymer matrix, and the composite materials exhibited good thermal stability at temperatures up to 200 °C. The acidized PMTDPABQ/G composites exhibited better TE performance than the ammoniated PMTDPABQ/G composites. The highest TE figure of merit, ZT = 5.32×10^{-3}, was obtained using acidized PMTDPABQ/G and was approximately 3 times greater than that of polythiophene (PTh)/G (1.37×10^{-3}).

Keywords: Conducting polymer, graphite, composite materials, thermoelectric property

1. Introduction

Recently, thermoelectric (TE) materials have received a great deal of attention because of their unique ability to convert heat into electricity without any moving parts or bulk fluids and vice versa.[1] The energy conversion efficiency of TE materials is determined by their TE figure of merit, $ZT = S^2\sigma T/K$, where S is the Seebeck coefficient, σ is the electrical conductivity, K is the thermal conductivity, and T is the absolute temperature. Inorganic materials such as bismuth telluride,[2] SrTe-PbTe,[3] and $Cu_{2-x}Se$[4-5] have been extensively studied for several years because of their relatively high ZT value. However, these materials also possess clear disadvantages such as poor processability, toxicity, brittleness, and high cost, which have impeded their widespread use as energy materials. In contrast, polymeric materials possess unique features that are useful in applications as TE materials such as low cost, ease of synthesis, solution processability over a wide range of parameter values,[6] and an intrinsically low thermal conductivity. Following the initial discovery of conducting polymers in the late 1970s,[7] polymers such as polyaniline[8-9], polythiophene, polyacetylene, polypyrrole and their derivatives[10] have received increasing attention as prospective TE materials. If the TE power factor ($P = S^2\sigma$) of conductive polymers could be substantially improved, these materials could be used in many TE applications. Unfortunately, the electrical conductivity and Seebeck coefficients of polymers are strongly negatively correlated.

The key to promoting the power factor and ZT of organic materials is to counteract the trade-off between the electrical conductivity and the Seebeck

coefficient. Many researchers have attempted to solve this problem by preparing polymer-inorganic TE composites.[10-11] One of the most attractive features of polymer-inorganic TE composites is the synergistic combination of the low thermal conductivity of polymers and the excellent conductivity of inorganic materials. Yao et al.[12] prepared polyaniline/single-walled carbon nanotube hybrid nanocomposites by in situ polymerization and obtained a maximum power factor of 20 μw/mK.[2] Composites of poly(3-hexylthiophene) and single- and multi-walled carbon nanotubes were prepared and exhibited a competitive TE performance and a high ZT > 10^{-2} at room temperature.[13] Adding tellurium particles, bismuth telluride particles, and carbon black to carbon fiber epoxy-matrix composites greatly increased the ZT of these composites from 9×10^{-6} to 9×10^{-2} at 343 K.[14] Polyaniline/$Ca_3Co_4O_9$ bulk composites fabricated by ball milling and hot -pressing have also been extensively studied.[15] Song et al.[16] prepared layered nanostructures of PDOT:PSS/SWCNTs (single-walled carbon nanotubes) by a two-step spin casting method and obtained a maximum power factor of 21.1 μW/mK.[2] Enhanced TE properties were measured for a series of expanded polymer graphite composite films.[17] Our group has also studied polyaniline/G composites, which were observed to exhibit a ZT of 1.37×10^{-3} at 393 K.[18]

The advances in polymer TE materials described above have been groundbreaking but limited in scope; indeed, this field is still in its infancy. Materials with improved TE properties could be produced by synthesizing novel conducting polymers with high Seebeck coefficients that could then be used to prepare

polymer-inorganic TE composites. In this study, PMTDPABQ was successfully synthesized because of its ease of preparation, small band gap, and potentially high Seebeck coefficient.[19] After PMTDPABQ was prepared, it was treated with HCl and ammonia. Graphite (G) was blended with acidized (Ac) PMTDPABQ and ammoniated (Am) PMTDPABQ by mechanical ball milling and cold pressing due to graphite's high conductivity, unique physical and chemical properties[17]. At the same time, G possesses a large surface area and can form strong interactions with polymer materials. Compared with other fillers, such as carbon nanotubes (CNTs), G may be expected to disperse easily in polymeric matrices. It is well known that interfacial interaction and dispersion are the key factors in evaluating polymer-based composites[20]. The effect of the G content on the TE properties of Ac PMTDPABQ/G and Am PMTDPABQ/G composites was investigated in detail. Polythiophene (PTh)/G composites were also prepared for comparison.

2. Experimental Section

2.1 Materials

Graphite with particle sizes in the 30 to 50 μm range, as measured by a laser particle size analyzer (Ls603), was obtained from commercial sources. Thiophene monomer, 3-methylthiophene and *p*-chloranil were purchased from Aladdin, Ltd. Anhydrous iron(III) chloride (CP) was obtained from Sinopharm Chemical Reagent Co. Ltd., and anhydrous chloroform (AR) was purchased from Shanghai Shenxiang Chemical Reagent Co. Ltd. Anhydrous chloroform and tetrahydrofuran (THF)

(Aldrich) were dried overnight using 4Å molecular sieves. Anhydrous 1,4-dioxane (Aldrich), 4-diphenylaminobenzaldehyde (Chemical Dynamics), 96% sulfuric acid (AR), hydrochloric acid (AR), ammonia (AR) and methanol (AR) were purchased from Guangzhou Donghong Chemical Reagent Co., Ltd. Ultrapure-grade nitrogen gas (Air Products) was used as received. All other reactive agents were used without further purification.

2.2 Preparation of PMTDPABQ

2.2.1 Preparation of poly[*(3-methylthiophene-2,5-diyl)(4-diphenylaminophenyl methane)*] *(PMTDPAB)*

3-Methylthiophene (2.45 g, 25 mmol), 4-diphenylaminobenzaldehyde (7.51 g, 28 mmol), 50 mL of *p*-dioxane, and 0.8 mL (15 mmol) of 96% sulfuric acid were added to a 250-mL, three-neck, round-bottom flask fitted with a condenser and a gas inlet and outlet. The polymerization reaction was carried out with stirring under a nitrogen atmosphere. The temperature was maintained at 85 °C for 28 h using an oil bath. A navy-blue product was precipitated by adding 500 mL of methanol dissolved in THF. The product was re-precipitated in methanol, recovered, and dried in a vacuum oven at 50 °C for 12 h.

^{1}H NMR ($CDCl_3$, δ, ppm, $SiMe_4$ as reference): 1.64-2.07 (s, 6H, 2(CH_3)), 5.74 (s, 2H, C(R)H), 7.01-7.32 (m, 28H, phenyl), 7.67 (d, J = 11 Hz, 2H, thiophene).

2.2.2 Preparation of PMTDPABQ

The reaction mixture was composed of 1.55 g of PMTDPAB, 1.08 g of *p*-chloranil, and 40 mL of anhydrous THF. The reaction was maintained at 50 °C for 8 h. The dark-blue reaction solution was poured into 100 mL of methanol while stirring, and the precipitate was recovered, filtered through a Büchner funnel, and then dissolved in chloroform. The filtrate was dried in an oven at 70 °C for 24 h.

^{1}H NMR ($CDCl_3$, δ, ppm, $SiMe_4$ as reference): 1.59-2.08 (s, 6H, 2(CH_3)), 6.61-7.63 (m, 28H, phenyl), 7.64 (d, J = 5.5 Hz, 2H, thiophene),

2.2.3 Preparation of Ac and Am PMTDPABQ

The resulting mass of PMTDPABQ was divided into two batches of 1.20 g each and then soaked in 2 M aqueous ammonia and 2 M HCl, respectively, for 8 h. The products were washed with deionized water and then dried in a vacuum oven at 60 °C.

2.3 Preparation of Ac and Am PMTDPABQ/G Composites

To promote mixing during the milling process, the PMTDPABQ and G powders were combined with 200 mL anhydrous ethanol at different G weight percentages and first ultrasonicated for 30 min, followed by mechanical blending at 1500 rpm for another 30 min. After filtering, the powder mixtures were dried at 60 °C for 24 h and then milled in an agate mortar for 1 h. Finally, the powder samples were milled in a 250-mL cylindrical steel jar with five 10-mm diameter steel balls and ten 5-mm diameter steel balls at a rotational speed of 270 rpm for 10 h.

2.4. Preparation of PTh/G composites

The PTh powder was chemically polymerized by oxidizing the monomer with $FeCl_3$ in anhydrous chloroform following a previously reported method[21]. The PTh/G composites were prepared using the same method as that used to prepare the Ac and Am PMTDPABQ/G composites.

2.5 Characterization

The Seebeck coefficients of the intrinsic polymers at various test temperatures were measured using Seebeck coefficient measurement systems by the temperature gradient method (ΔK=10 K) at temperatures ranging from 303 K to 363 K. The morphologies of the bulk samples were observed using scanning electron microscopy (SEM, Hitachi S-4700). Powders with different G contents were dispersed in KBr disks, and their Fourier transform infrared spectra (FTIR) were recorded on a Fourier transform infrared spectrometer (IFS 120HR, Bruker). The phases of the composites were characterized by X-ray diffraction (XRD) using a Bruker D8 Advance X-ray diffractometer with Cu Kα radiation. Thermal gravimetric analysis (TGA) was conducted on a TGA-Q50 (USA) from room temperature to 600 °C at a heating rate of 10 °C min^{-1} under a nitrogen flow of 40 mL min^{-1} to examine the thermal stability of the materials. Raman spectra were collected using a Raman spectrometer (RENISHAW, λ_{exc}=514.5 nm). The carrier concentration and Hall mobility were measured by an ET-9007 Hall measurement system through the van de Pauw method.

The electric conductivities and Seebeck coefficients of the bulk composites were simultaneously measured using a Seebeck coefficient/electric conductivity measuring system (ZEM-2, ULVAC-RIKO, Japan) from 303 K to 393 K in a helium atmosphere. The thermal conductivity was measured using a thermal conductivity tester (KY-DRX-RW, Shanghai). A cuboid specimen with dimensions of 16.0 mm × 5.10 mm × 3.0 mm was prepared under a pressure of 15 MPa for electrical properties measurement, and a disk specimen with a diameter of 15.0 mm and a height of 3.0-4.0 mm was prepared under a pressure of 20 MPa for thermal conductivity and Hall effect measurements. The densities of the cuboid specimen and disk specimen were approximately ~1.84 g/cm^3 and ~1.86 g/cm^3, respectively.

3. Results and discussion

3.1 Synthesis and Seebeck Coefficient of PMTDPABQ

The polymer synthesis process is outlined in Scheme 1. PMTDPAB containing a thiophene ring structure and bulky side groups was synthesized by a coupling reaction between 3-methylthiophene and 4-diphenylaminobenzaldehyde. The polymerization was carried out using chemical oxidation with concentrated sulfuric acid as the oxidant. This polymer is more soluble in organic solvents than other previously studied polythiophenes and their derivatives,[22] most likely because of the presence of diphenylaminobenzylidene side groups. The polymer was then dehydrogenated to produce PMTDPABQ with a small band gap.[19] The diphenylaminobenzylidene side group served as an electron donor to narrow the band gap of the polymer.[23] A

conducting polymer with a small band gap facilitates doping to obtain intrinsic metallic conductivity. Moreover, polymers formed with side groups containing nitrogen atoms can be doped with HCl or $NH_3 \cdot H_2O$, resulting in Ac PMTDPABQ and Am PMTDPABQ, respectively. The properties of these polymers and their composites were investigated.

Fig. 1 shows the ^{1}H NMR spectra of the obtained PMTDPAB and PMTDPABQ products. The presence of a $N(C_6H_4)_2$ group on the conjugated structure of the benzene ring and the alkyl group was shown to reduce the chemical shift in hydrogen atoms on the thiophene ring (δ =7.64). No absorption peaks were observed in the ^{1}H NMR spectra at δ = 5.7 for the hydrogen atoms on the thiophene and benzene rings connected to the methine bridge carbon -CH- of PMTDPABQ, demonstrating that PMTDPAB was completely dehydrogenated. Unlike polymers reported in the literature,[19, 24] all of the PMTDPABQ products were converted to poly(thiophene methine) structures. This result was obtained because the diphenylaminobenzylidene side group enhanced the degree of dehydrogenation. There was a significant difference after the dehydrogenation of PMTDPAB. A clear peak for PMTDPAB in the ^{1}H NMR was observed at δ = 5.7, from which a degree of dehydrogenation of approximately 15.1% was estimated.

Fig. 2 shows the FT-IR spectra of PMTDPAB, Ac PMTDPABQ, and Am PMTDPABQ. The primary absorption peaks for PMTDPAB and PMTDPABQ were observed. The peaks in the 3000-3100 cm^{-1} range were assigned to phenyl and thiophene C-H stretching vibrations. The small peak at 2858 cm^{-1} is characteristic of

the stretching vibrations that are associated with the -CH_3 group.[19] The sharp strong peak at 1600 cm^{-1} was attributed to benzene ring C=C stretching vibrations.[23, 25] The peaks at 1120 cm^{-1} and 810 cm^{-1} were attributed to the in-plane and out-of-plane aromatic C-H bending vibrations of the 1,4-disubstituted aromatic ring.[26] For the Ac PMTDPABQ and Am PMTDPABQ powders, the band at 1670 cm^{-1} resulted from the C=C stretching of a quinoid structure,[27] indicating the existence of a conjugated main chain. The small peak at 2330 cm^{-1} was assigned to Ac PMTDPABQ and was associated with the NH^+ vibration of the -$C_6H_4NH^+(C_6H_4)_2$- group.[28] For the PMTDPAB powder, no peak was clearly associated with a quinoid structure, most likely because the quinone was not completely dehydrogenated, in agreement with the ^{1}H NMR data.

Fig. 3 shows the Seebeck coefficients of PTh and Ac and Am PMTDPABQ. The Seebeck coefficient of Ac PMTDPABQ was high (> 157 μV/K) and increased slightly with temperature. However, the Seebeck coefficient of Am PMTDPABQ was relatively low at lower temperatures (approximately 104 μV/K at 317 K) and decreased as the temperature increased. At 363 K, the Seebeck coefficient of Ac PMTDPABQ was 178 μV/K, whereas the Seebeck coefficient for Am PMTDPABQ was only 22 μV/K. These differences may be due to different carrier concentrations and carrier mobilities. Ac PMTDPABQ can provide a sufficient amount of H^+ to increase the carrier concentration and can also improve carrier mobility due to its stretched molecular chain conformation[29]. Increasing the carrier concentration generally increases the electrical conductivity and decreases the Seebeck coefficient,

whereas a higher Seebeck coefficient can be obtained by increasing the carrier mobility.[10, 30-31] Thus, we hypothesize that the carrier mobility has a greater effect on the Seebeck coefficient than the carrier concentration, resulting in Ac PMTDPABQ having a higher Seebeck coefficient than Am PMTDPABQ, which could be indirectly confirmed by the data shown in Table 1. Pure polymer samples, which possessed a high resistance beyond the measuring range of the test equipment, were not examined. As shown in Table 1, Ac PMTDPABQ-related composites exhibited both higher carrier concentrations and carrier mobilities than those of Am PMTDPABQ-related composites. The Seebeck coefficient of PTh was always much lower than that of Ac PMTDPABQ: the Seebeck coefficient of PTh at 323 K was 64 μV/K, which was approximately half that of Ac PMTDPABQ (158 μV/K).

3.2 SEM, TGA, XRD and Raman analysis of PMTDPABQ/G composites

Fig. 4 shows the morphologies of cross-sections of the Am PMTDPABQ (1), Ac PMTDPABQ (5), and Am PMTDPABQ/G composites with G contents of 20% (2), 40% (3), and 50% (4) and of Ac PMTDPABQ with G contents of 20% (6), 40% (7), and 70% (8). The cross-sections of the bulk samples were obtained by quenching and fracturing. In Fig. 4, the polymer matrix appears as a layered structure to which small particles were adhered and G shows a flake-like morphology. Fig. 4 (1, 5) shows that the Am PMTDPABQ surfaces were much smoother than those of Ac PMTDPABQ. This result may be attributed to the smaller distances between the main chains of Am PMTDPABQ.[29] For all of the composite samples, the flake-shaped G component was

evenly dispersed in the dark background of the polymer matrix. Further analysis of the composites with a low G content yielded improved combinations of the matrix and the filler, as shown in Fig. 4 (2, 3, 4, 6, and 7). An excessively high G content weakened the interfaces between the matrix and filler, thereby decreasing the TE performance most likely because the Seebeck coefficient decreased.

Thermal gravimetric analysis (TGA) measurements were conducted under a nitrogen flow rate of 40 mL/min from room temperature to 600 °C at a heating rate of 10 °C/min. The TGA results are shown in Fig. 5. Ac and Am PMTDPABQ and their composites exhibited excellent thermal stability. Dramatic weight loss was observed for the PMTDPABQ/G composites above 200 °C, indicating the decomposition of the PMTDPABQ powder. The weight loss also decreased as the G content increased. The Am PMTDPABQ/G composites with a G content below 40% had a decomposition temperature of approximately 210 °C, which increased to approximately 260 °C for a G content over 50%. The high thermal stability and the uniform dispersion of G increased the thermal stability of the composites.[32] The results indicate that the TE properties of the composites could be studied below 200 °C without destroying the PMTDPABQ structures.

Fig. 6 shows the XRD patterns of Ac and Am PMTDPABQ and their composites at room temperature. Prominent scattering at Bragg angles of $2\theta = 26.6°$ and $2\theta = 55°$ were observed, which was attributed to G.[33] The intensity of the two peaks grew as the G concentration increased. However, the position of the peaks remained unchanged, suggesting that no chemical reaction occurred between the polymer and G, and the Ac

and Am PMTDPABQ structures did not change during the blending procedure. Fig. 6 shows magnified patterns of Ac and Am PMTDPABQ. The broad diffraction peak at approximately 2θ = 23° corresponds to Am PMTDPABQ, indicating an amorphous structure.[21] The spectra for the Ac PMTDPABQ powder exhibited sharp well-defined diffraction peaks at 2θ = 26.42° and 2θ = 32.23°, indicating a low level of crystallinity for the polymer,[27] which could help increase the conductivity of the polymer's composites.

The Raman spectra of the pure polymer and polymer-based composites are shown in Fig. 7. For the pure Ac PMTDPABQ powder, the spectrum shows several characteristic peaks. C-H bending of the benzenoid ring (~1170 cm^{-1}), C-N stretching (~13500cm cm^{-1}), C-C stretching of the benzenoid rings (~1592 cm^{-1})[12] and C=C stretching of the quinoid ring (~1492 cm^{-1}) were observed. Previous Raman studies on polymer/graphene have demonstrated that strong π-π conjugation interactions cause a red shift of the characteristic peaks of the corresponding polymer[34,35]. As shown in Fig. 7, the peaks at 13500 cm^{-1} and 15922 cm^{-1} of Ac PMTDPABQ shifted to lower frequencies after the addition of G. The same tendency was observed for Am PMTDPABQ. Raman spectra provide evidence of the existence of π-π conjugation interactions between PMTDPABQ and G.

3.3 Comparison of TE performances among PMTDPABQ/G and PTh/G composites

Fig. 8 presents the Seebeck coefficients for the Ac PMTDPABQ/G and Am

PMTDPABQ/G composites at different temperatures. As the G content increased, the Seebeck coefficient of the composites gradually decreased. The Ac PMTDPABQ/G composites exhibited a higher Seebeck coefficient than that of the Am PMTDPABQ/G composites. At 20 wt% G, the Ac PMTDPABQ/G composite had a Seebeck coefficient of 43.8 μV/K, whereas the Am PMTDPABQ/G composite had a Seebeck coefficient of 20.5 μV/K at 393 K, which was approximately half that of the coefficient for the Ac PMTDPABQ/G composite. Increasing the G content created more conductive paths in the composites,[21] which had a strong effect on the Seebeck coefficient. Increasing the G content also resulted in a loss of polymer content, which enhanced the carrier mobility of the composites and reduced the large number of interfaces between the polymer matrix and G, thereby decreasing the Seebeck coefficient of the composites. Fig. 9 shows that the Seebeck coefficient of the PTh/G composites decreased from 31.1 μV/K to 9.1 μV/K as the G content increased. This trend was similar to that observed for the Ac PMTDPABQ/G and Am PMTDPABQ/G composites. As shown, the Seebeck coefficient of the Ac PMTDPABQ/G composites is clearly much higher than that of the PTh/G composites. The high Seebeck coefficient of the Ac PMTDPABQ/G composites could primarily be attributed to the high Seebeck coefficient of Ac PMTDPABQ. We conclude that the polymers with high Seebeck coefficients can improve the TE performance of polymer-inorganic composites.

Fig. 10 shows the electrical conductivity of the Ac PMTDPABQ/G and Am PMTDPABQ/G composites. The electrical conductivity of all of the samples

increased with the G content. The Ac PMTDPABQ/G composites exhibited slightly higher electrical conductivity than did the Am PMTDPABQ/G composites. At 303 K, the highest conductivity (5.66×10^4 S/m) of the Ac PMTDPABQ/G composites was obtained for a 90 wt% G loading. It is known that G can serve as a π-ligand,[34-35] and there are many conjugated structures in the main chains of PMTDPABQ. Furthermore, π electrons have a strong tendency to delocalize to other adjacent conjugated structures.[26, 36] Thus, a π electron of G can interact with the conjugated structure of PMTDPABQ during ball milling to produce a larger conjugated structure that can act as a conductive unit. At low graphite loadings, these conductive units are separated from each other. With increasing G content, these units are gradually connected together to form a conductive network that rapidly enhances the electrical conductivity of the composites. Fig. 11 shows that increasing the G content from 10 to 80 wt% at 393 K greatly improved the electrical conductivity of the PTh/G composites from 1.88×10^2 S/m to 4.78×10^4 S/m. The electrical conductivity of the PTh/G composites was clearly lower than the conductivities of the Ac PMTDPABQ/G and Am PMTDPABQ/G composites. At 393 K and a 50 wt% G loading, the electrical conductivity of the PTh/G composites was 6.51×10^3 S/m, whereas that of the Ac PMTDPABQ/G composites was 1.092×10^4 S/m.

The thermal conductivity of the composites was determined to obtain the ZT values of the Ac PMTDPABQ/G, Am PMTDPABQ/G, and PTh/G composites. The results are shown in Fig. 12. The thermal conductivity of all of the samples increased with the G content. All of the composites showed relatively low thermal conductivity

for various G contents, which was approximately an order of magnitude lower than the thermal conductivities of inorganic TE materials (1-10 W/mK). Low thermal conductivities can enhance TE performance.

The performances of the TE materials were determined based on the ZT values. The experimental results that are depicted in Figs. 8 to 12 were used to calculate and plot the ZT values (see Figs. 13 and 14). Fig. 13 shows that the Ac PMTDPABQ/G composites exhibited higher ZT values than those of the Am PMTDPABQ/G composites at the same G content. The highest ZT value (5.32×10^{-3}) for the Ac PMTDPABQ/G composites was obtained at 363 K for a 90 wt% G loading. Fig. 14 shows that the highest ZT value of PTh/G was 1.37×10^{-3} at 333 K for a 40 wt% G loading, which was 3 times lower than that of the Ac PMTDPABQ/G composites.

4. Conclusions

Ac and Am PMTDPABQ/G composites were successfully prepared in this study. The TE properties of the composites were investigated in detail as a function of the G content. Increasing the G content of the Ac and Am PMTDPABQ/G composites significantly improved their ZT values. The Ac PMTDPABQ/G composites exhibited better TE properties than traditional conductive PTh polymers blended with G. The highest ZT (5.32×10^{-3}) for Ac PMTDPABQ/G was obtained at a 90 wt% G content, which was approximately 3 times greater than that of the PTh/G composites (1.37×10^{-3}). These results suggest that synthesizing novel conductive polymers with high Seebeck coefficients may be an excellent means of improving the TE

performance of polymer-inorganic composites.

Acknowledgements

The authors would like to acknowledge the financial support of the National Natural Science Foundation of China (Nos. 51003060, 51171117, and 51101103) and the Shenzhen Sci & Tech (Research grants JC2011042 100070A and ZYC201105170225A). W.-Y. Wong acknowledges the financial support from Hong Kong Baptist University (FRG2/12-13/083), Hong Kong Research Grants Council (HKBU203313) and Areas of Excellence Scheme, University Grants Committee of HKSAR, China (Project No. AoE/P-03/08). H. Li thanks the 111 Project and Beijing Engineering Research Center of Food Environment and Public Health from Minzu University of China (No. B08044 and No.10301-01404026) for financial support. The work was also supported by Partner State Key Laboratory of Environmental and Biological Analysis and Strategic Development Fund of HKBU.

References and Notes

1. He M, Qiu F, Lin Z. Towards high-performance polymer-based thermoelectric materials. Energy & Environmental Science 2013;6:1352.
2. Zhao XB, Ji XH, Zhang YH, Zhu TJ, Tu JP, Zhang XB. Bismuth telluride nanotubes and the effects on the thermoelectric properties of nanotube-containing nanocomposites. Appl Phys Lett 2005;86.
3. Biswas K, He J, Blum ID, et al. High-performance bulk thermoelectrics with all-scale hierarchical architectures. Nature 2012;489:414-8.
4. Li D, Qin XY, Liu YF, et al. Chemical synthesis of nanostructured Cu2Se with high thermoelectric

performance. Rsc Adv 2014;4:8638-44.

5. Liu H, Shi X, Xu F, et al. Copper ion liquid-like thermoelectrics. Nat Mater 2012;11:422-5.

6. Bubnova O, Khan ZU, Malti A, et al. Optimization of the thermoelectric figure of merit in the conducting polymer poly(3,4-ethylenedioxythiophene). Nat Mater 2011;10:429-33.

7. Shirakawa H, Louis EJ, Macdiarmid AG, Chiang CK, Heeger AJ. Synthesis of Electrically Conducting Organic Polymers - Halogen Derivatives of Polyacetylene, (Ch)X. J Chem Soc Chem Comm 1977:578-80.

8. Wang WJ, Sun SP, Gu SJ, et al. One-pot fabrication and thermoelectric properties of Ag nanoparticles-polyaniline hybrid nanocomposites. Rsc Adv 2014;4:26810-6.

9. Ansari MO, Khan MM, Ansari SA, Lee J, Cho MH. Enhanced thermoelectric behaviour and visible light activity of Ag@TiO2/polyaniline nanocomposite synthesized by biogenic-chemical route. Rsc Adv 2014;4:23713-9.

10. Du Y, Shen SZ, Cai KF, Casey PS. Research progress on polymer-inorganic thermoelectric nanocomposite materials. Progress in Polymer Science 2012;37:820-41.

11. Dubey N, Leclerc M. Conducting Polymers: Efficient Thermoelectric Materials. J Polym Sci Pol Phys 2011;49:467-75.

12. Yao Q, Chen LD, Zhang WQ, Liufu SC, Chen XH. Enhanced Thermoelectric Performance of Single-Walled Carbon Nanotubes/Polyaniline Hybrid Nanocomposites. Acs Nano 2010;4:2445-51.

13. Bounioux C, Diaz-Chao P, Campoy-Quiles M, et al. Thermoelectric composites of poly(3-hexylthiophene) and carbon nanotubes with a large power factor. Energy & Environmental Science 2013;6:918-25.

14. Han SJ, Chung DDL. Carbon fiber polymer-matrix structural composites exhibiting greatly

enhanced through-thickness thermoelectric figure of merit. Compos Part a-Appl S 2013;48:162-70.

15. Zheng B, Lin YH, Lan JL, Yang XP. Thermoelectric Properties of Ca3Co4O9/Polyaniline Composites. J Mater Sci Technol 2014;30:423-6.

16. Song HJ, Liu CC, Xu JK, Jiang QL, Shi H. Fabrication of a layered nanostructure PEDOT:PSS/SWCNTs composite and its thermoelectric performance. Rsc Adv 2013;3:22065-71.

17. Piao MX, Kim G, Kennedy GP, Roth S, Dettlaff-Weglikowska U. Preparation and characterization of expanded graphite polymer composite films for thermoelectric applications. Phys Status Solidi B 2013;250:2529-34.

18. Wang L, Wang DG, Zhu GM, Li JQ, Pan F. Thermoelectric properties of conducting polyaniline/graphite composites. Materials Letters 2011;65:1086-8.

19. Chen WC, Jenekhe SA. Small-Bandgap Conducting Polymers Based on Conjugated Poly(Heteroarylene Methines) .1. Precursor Poly(Heteroarylene Methylenes). Macromolecules 1995;28:454-64.

20. Cai DY, Song M. Recent advance in functionalized graphene/polymer nanocomposites. J Mater Chem 2010;20:7906-15.

21. Wang L, Jia XL, Wang DG, Zhu GM, Li JQ. Preparation and thermoelectric properties of polythiophene/multiwalled carbon nanotube composites. Synthetic Met 2013;181:79-85.

22. Chan HSO, Ng SC. Synthesis, characterization and applications of thiophene-based functional polymers. Progress in Polymer Science 1998;23:1167-231.

23. Gao C, Wu H, Yi W, Li B. Synthesis and Characterization of Small Bandgap Conjugated Polymer:Poly{ 3-octylthiophen-2,5-diyl - p-(N,N-dimethylamino)benzyliden equinomethane }. Fine Chemicals 2004;21:249-52.

24. Jenekhe SA. Synthesis and Characterization of Carbon-Atom Bridged Heterocyclic Polymers of Specified Conjugation Length .1. Novel Polyterthiophenes. Macromolecules 1990;23:2848-54.

25. Zhang Z, Wu H, Yi W. SYNTHESIS AND CHARACTERIZATION OF POLY (3-ACETYL) PYRROLE-2,5-DIYL(p-NITROBENZYLIDENE). Acta Polymerica Sinica 2004;0:528-33.

26. Zeng XR, Ko TM. Structures and properties of chemically reduced polyanilines. Polymer 1998;39:1187-95.

27. Khuspe GD, Chougule MA, Navale ST, Pawar SA, Patil VB. Camphor sulfonic acid doped polyaniline-tin oxide hybrid nanocomposites: Synthesis, structural, morphological, optical and electrical transport properties. Ceram Int 2014;40:4267-76.

28. Khuspe GD, Navale ST, Bandgar DK, Sakhare RD, Chougule MA, Patil VB. SnO(2)nanoparticles-modified Polyaniline Films as Highly Selective, Sensitive, Reproducible and Stable Ammonia Sensors. Electron Mater Lett 2014;10:191-7.

29. Ying LYS, Fu-Ping SQW. Thermoelectric Properties of Conducting Polyaniline Co-Doped with Hydrochloric Acid and Sulfosalicylic Acid. Chinese Journal of Inorganic Chemistry 2013;9:019.

30. Chatterjee K, Mitra M, Ganguly S, Kargupta K, Banerjee D. Thermoelectric Performance of Electrodeposited Nanostructured Polyaniline Doped with Sulfo-Salicylic Acid. J Appl Polym Sci 2014;131.

31. Wu JS, Sun YM, Xu W, Zhang QC. Investigating thermoelectric properties of doped polyaniline nanowires. Synthetic Met 2014;189:177-82.

32. Chen GX, Kim HS, Park BH, Yoon JS. Multi-walled carbon nanotubes reinforced nylon 6 composites. Polymer 2006;47:4760-7.

33. Han ZD, Wang JQ. XRD/XPS study on oxidation of graphite. Chinese Journal of Inorganic

Chemistry 2003;19:1366-70.

34. Berger C, Song ZM, Li TB, et al. Ultrathin epitaxial graphite: 2D electron gas properties and a route toward graphene-based nanoelectronics. J Phys Chem B 2004;108:19912-6.

35. Castro Neto AH, Guinea F, Peres NMR, Novoselov KS, Geim AK. The electronic properties of graphene. Rev Mod Phys 2009;81:109-62.

36. Shi W, Ye JT, Checkelsky JG, Terakura C, Iwasa Y. Transport Properties of Polymer Semiconductor Controlled by Ionic Liquid as a Gate Dielectric and a Pressure Medium. Adv Funct Mater 2014;24:2005-12.

Figure Captions

Table 1 Carrier concentration and carrier mobility of PMTDPABQ/G composites with 20% and 40% G contents

Scheme 1 Synthesis of PMTDPABQ

Fig. 1 ^{1}H NMR spectra of PMTDPABQ and PMTDPAB

Fig. 2 IR spectra of PMTDPAB, Ac PMTDPABQ, and Am PMTDPABQ

Fig. 3 Seebeck coefficients for PTh, Am and Ac PMTDPABQ at different temperatures

Fig. 4 Cross-sectional SEM images of Am PMTDPABQ (1), Ac PMTDPABQ (5), and their composites; Am PMTDPABQ/G composites with various G contents: 20% (2), 40% (3), and 50% (4); Ac PMTDPABQ with various G contents: 20% (6), 40% (7), and 70% (8)

Fig. 5 TGA curves for Ac and Am PMTDPABQ, Am PMTDPABQ/G, and Ac PMTDPABQ/G composites

Fig. 6 X-ray diffraction patterns of Ac and Am PMTDPABQ, Am PMTDPABQ/G, and Ac PMTDPABQ/G composites

Fig. 7 Raman spectra (λ_{exc}=514.5 nm) of Am PMTDPABQ, Ac PMTDPABQ powders and their composite powders

Fig. 8 Seebeck coefficients of Am PMTDPABQ/G and Ac PMTDPABQ/G composites at different graphite contents. The inset shows the variation in the Seebeck coefficient with temperature.

Fig. 9 Seebeck coefficients of PTh/G composites at different graphite contents.

The inset shows the variation in the Seebeck coefficient with temperature.

Fig. 10 Electrical conductivities of Am PMTDPABQ/G and Ac PMTDPABQ/G composites at different graphite contents

Fig. 11 Electrical conductivities of PTh/G composites at different graphite contents

Fig. 12 Thermal conductivities of PTh/G, Am PMTDPABQ/G, and Ac PMTDPABQ/G composites at different graphite contents

Fig. 13 ZT values of Am PMTDPABQ/G and Ac PMTDPABQ/G composites at different graphite contents

Fig. 14 ZT values of PTh/G composites at different graphite contents

Table 1 Carrier concentration and carrier mobility of PMTDPABQ/G composites with 20% and 40% G contents

Sample	Carrier concentration (cm^{-3})	Carrier mobility ($cm^2/V\ S$)
20% Am PMTDPABQ	7.69×10^{17}	13.29
20% Ac PMTDPABQ	7.86×10^{17}	13.49
40% Am PMTDPABQ	2.92×10^{19}	13.52
40% Ac PMTDPABQ	2.95×10^{19}	13.80

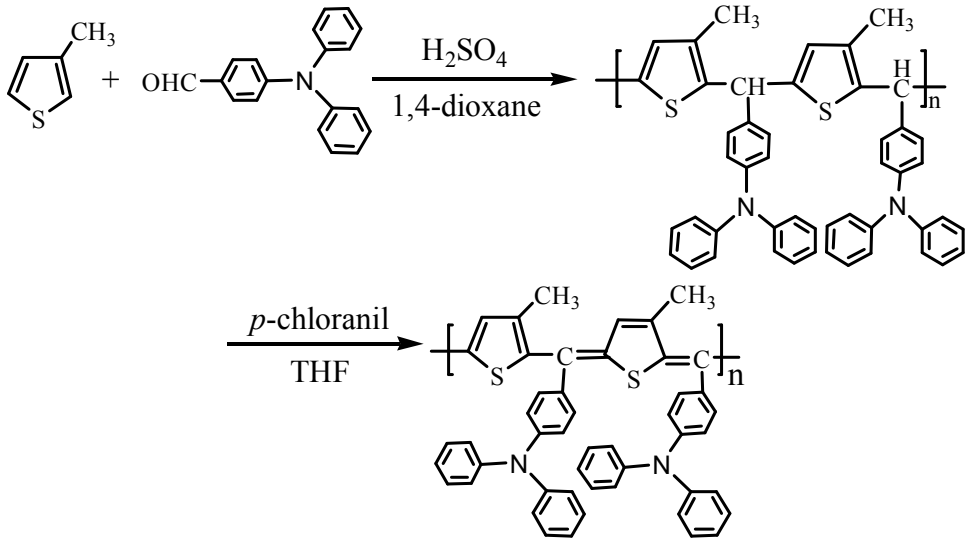

Scheme 1 Synthesis of PMTDPABQ

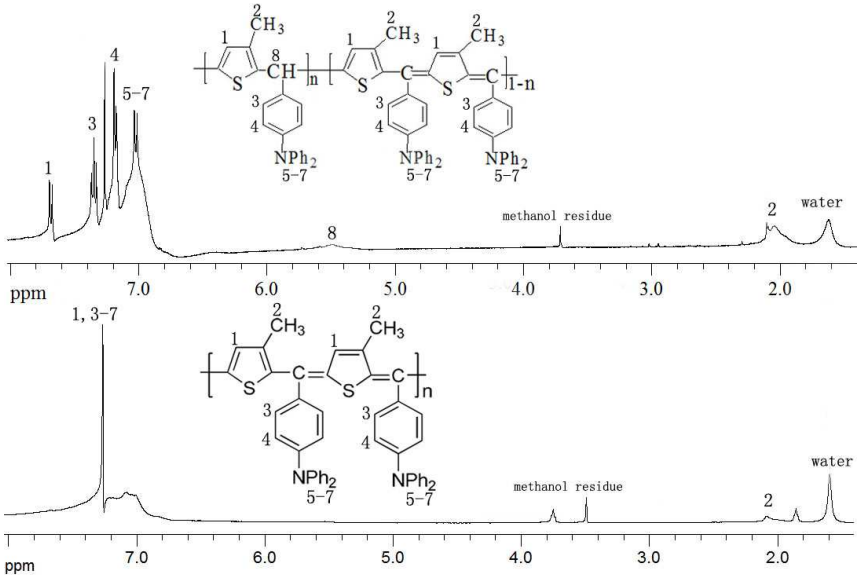

Fig. 1 ^{1}H-NMR spectra of PMTDPABQ and PMTDPAB

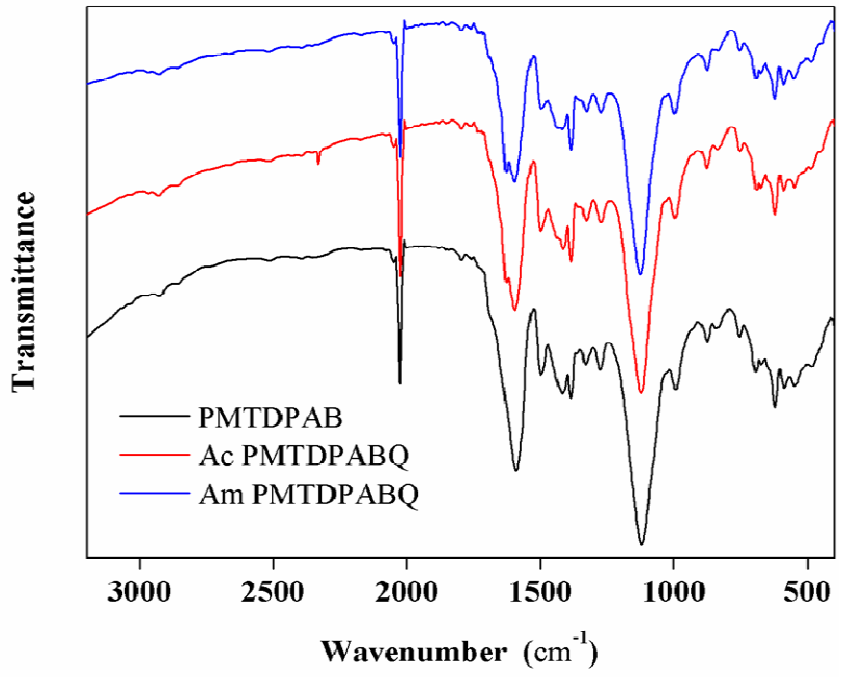

Fig. 2 IR spectra of PMTDPAB, Ac PMTDPABQ and Am PMTDPABQ

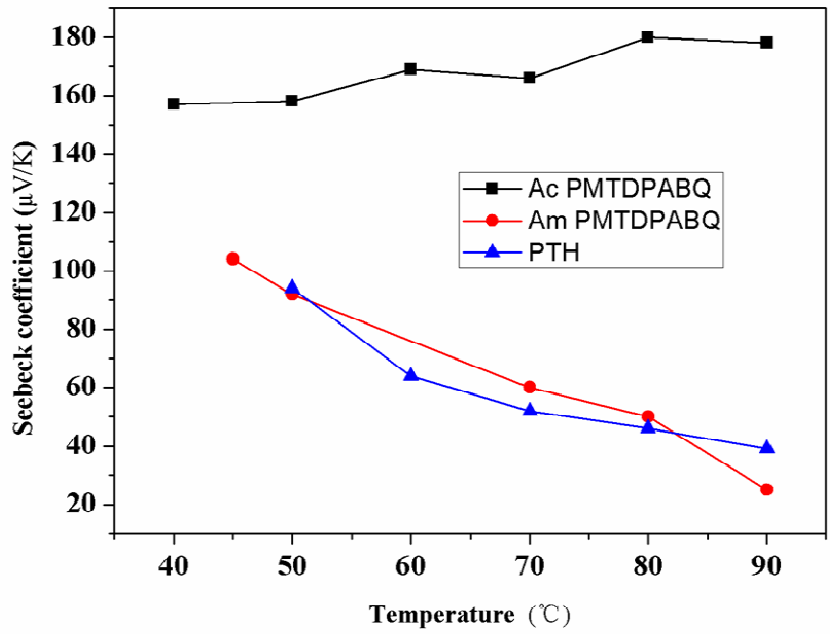

Fig. 3 Seebeck coefficients for PTh, Ac and Am PMTDPABQ at different temperatures

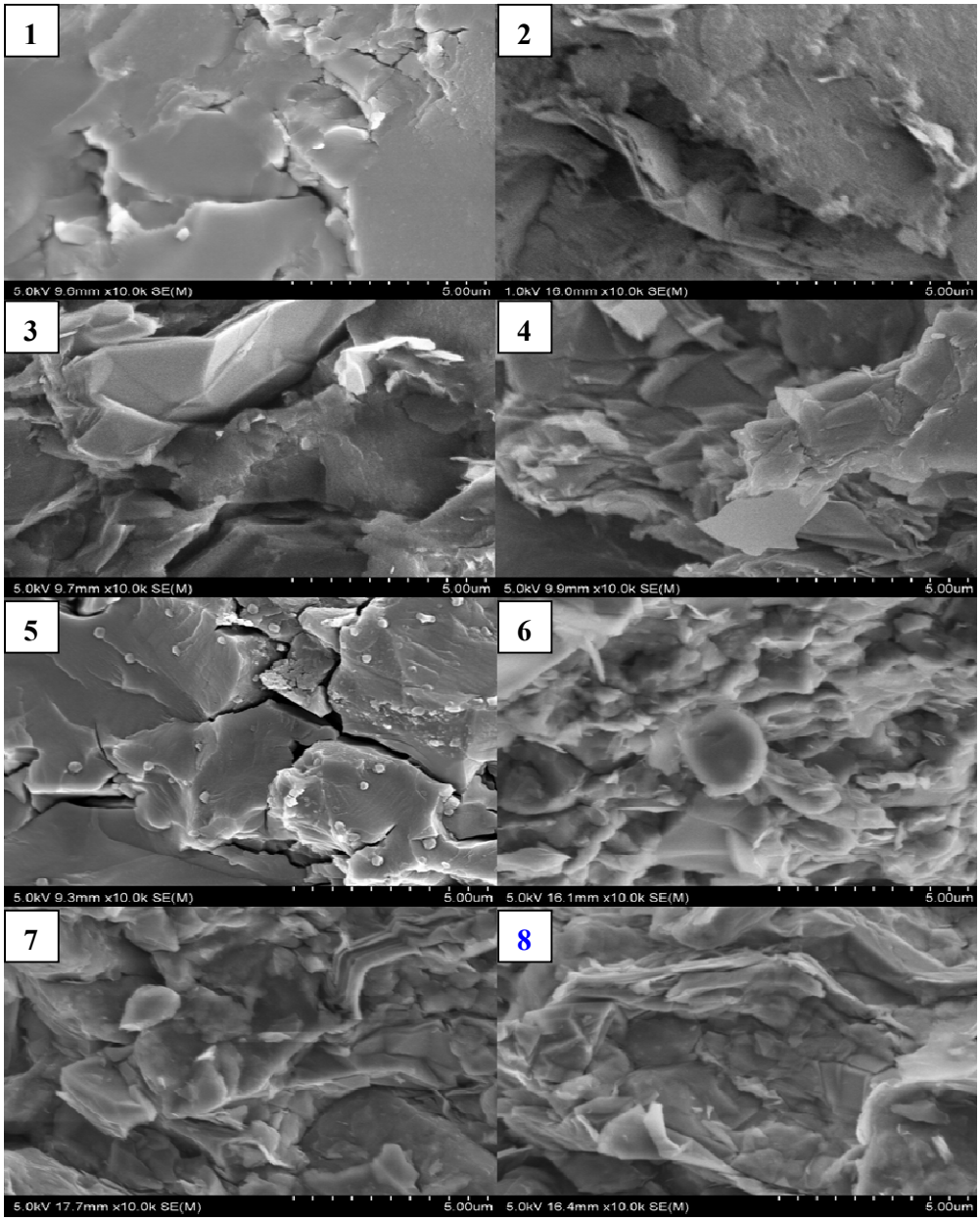

Fig. 4 Cross-sectional SEM images of Am PMTDPABQ (1), Ac PMTDPABQ (5), and their composites; Am PMTDPABQ/G composites with various G contents: 20% (2), 40% (3), and 50% (4); Ac PMTDPABQ with various G contents: 20% (6), 40% (7), and 70% (8)

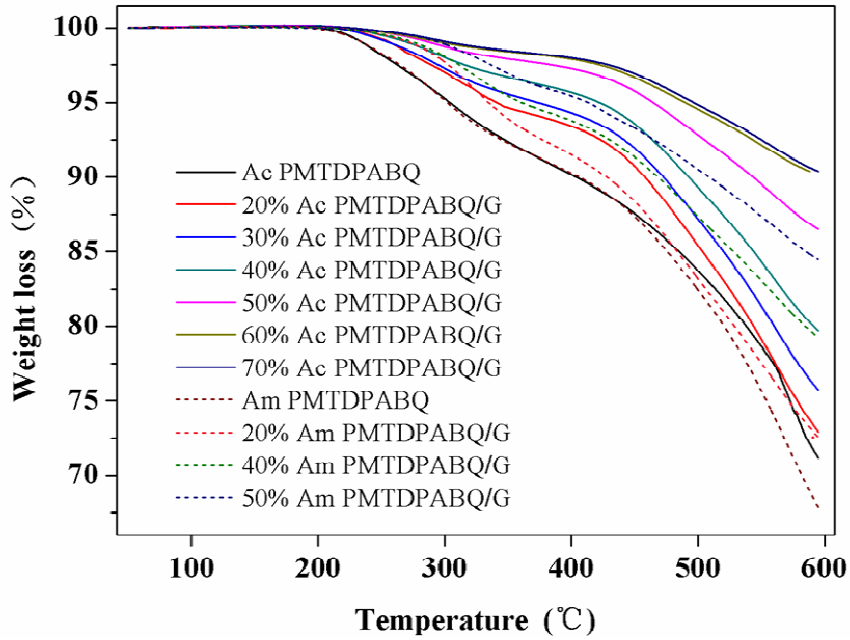

Fig. 5 TGA curves for Ac and Am PMTDPABQ, Am PMTDPABQ/G, and Ac PMTDPABQ/G composites

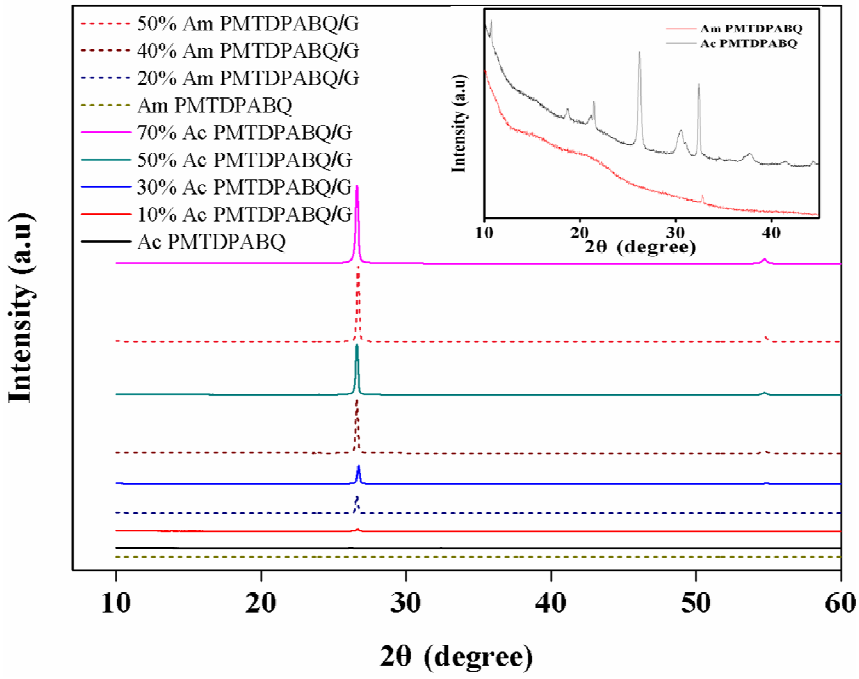

Fig. 6 X-ray diffraction patterns of Ac and Am PMTDPABQ, Am PMTDPABQ/G, and Ac PMTDPABQ/G composites

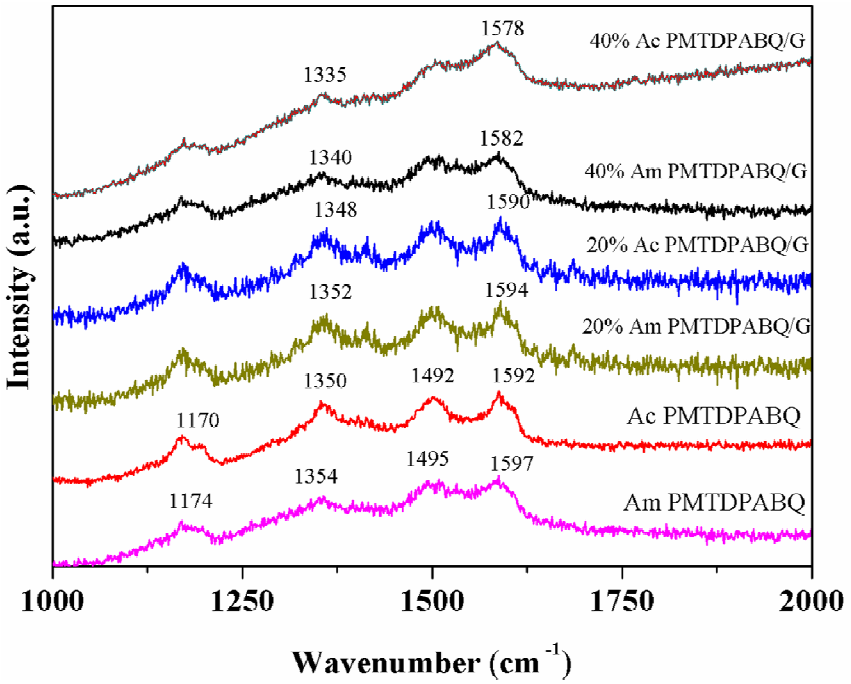

Fig. 7 Raman spectra n (λ_{exc}=514.5 nm) of Am PMTDPABQ and Ac PMTDPABQ powders and their composite powders

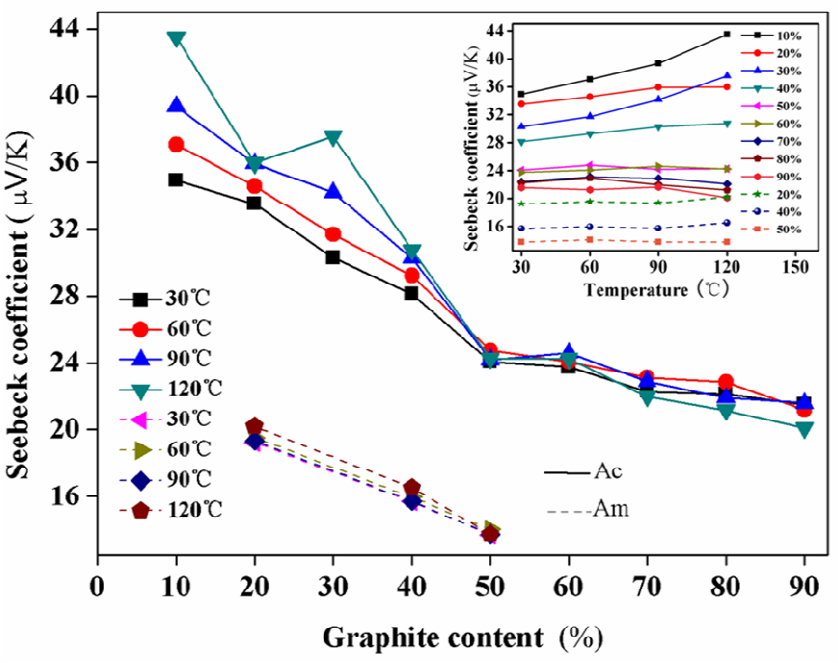

Fig. 8 Seebeck coefficients for Am PMTDPABQ/G and Ac PMTDPABQ/G composites at different graphite contents. The inset shows the variation in the Seebeck coefficient with temperature.

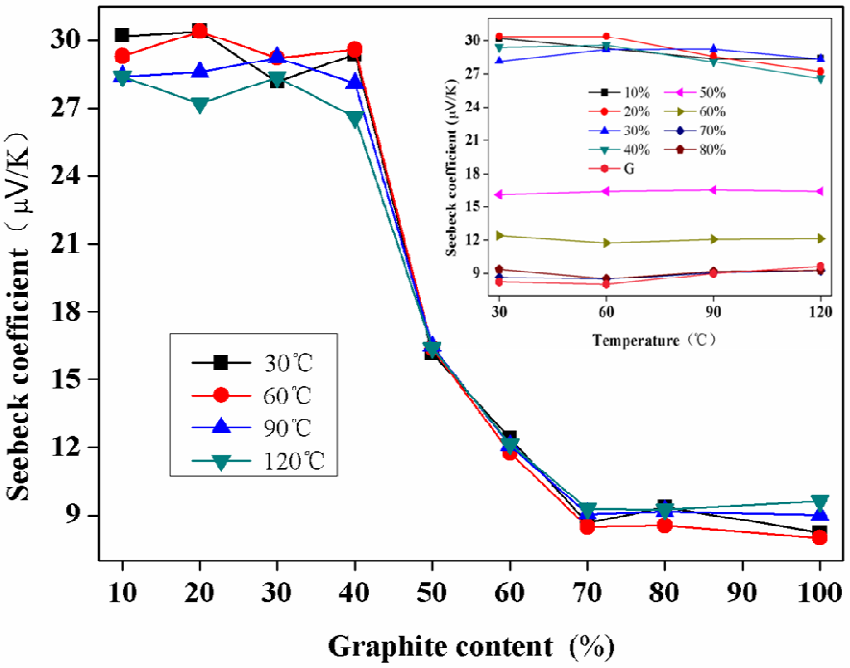

Fig. 9 Seebeck coefficients of PTh/G composites at different graphite content. The inset shows the variation in the Seebeck coefficient with temperature.

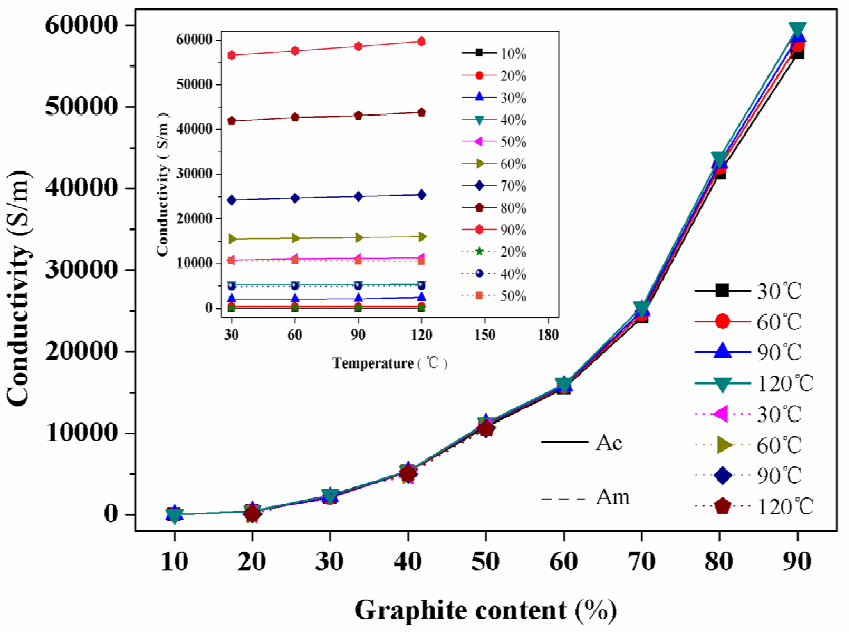

Fig. 10 Electrical conductivities of Am PMTDPABQ/G and Ac PMTDPABQ/G composites at different graphite contents

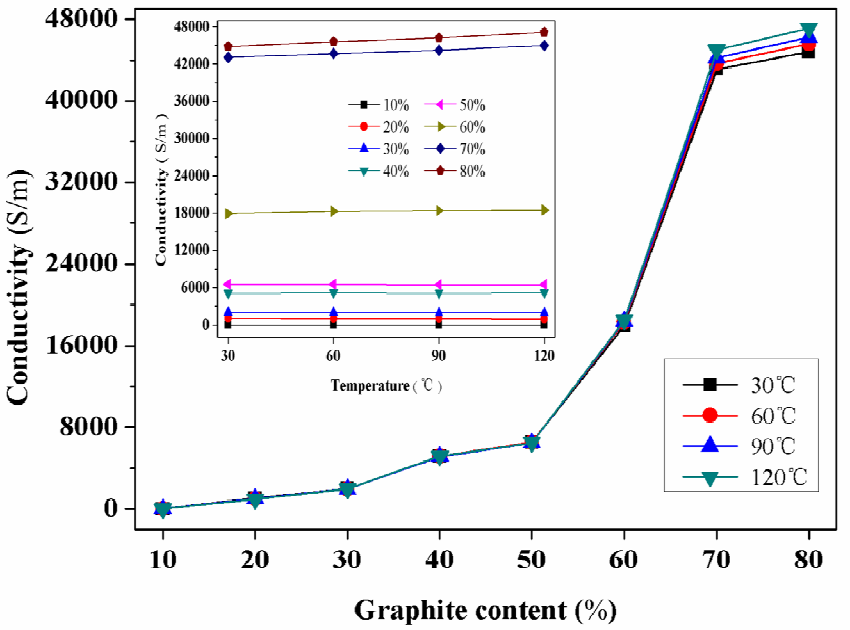

Fig. 11 Electrical conductivities of PTh/G composites at different graphite contents

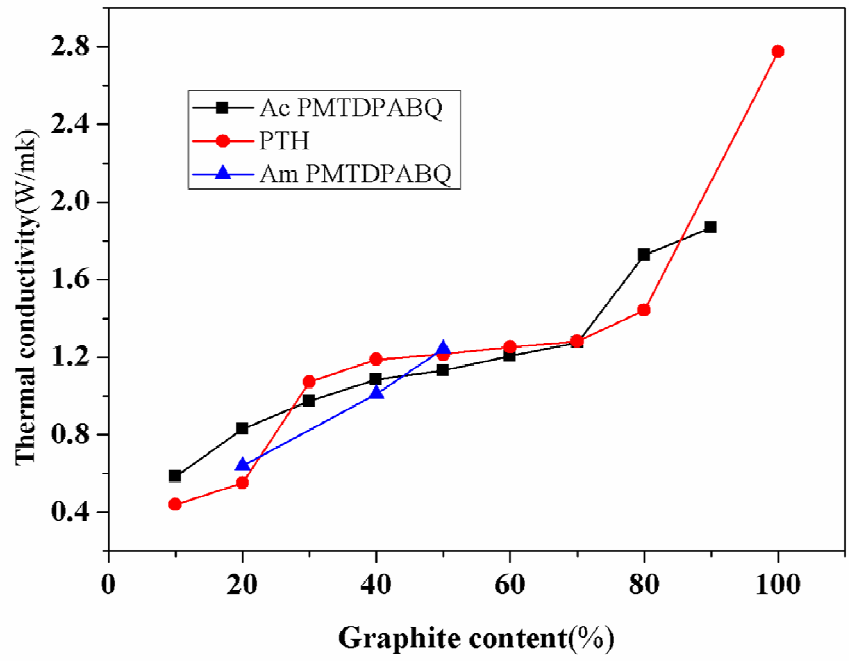

Fig. 12 Thermal conductivities of PTh/G, Am and Ac PMTDPABQ/G composites at different graphite contents

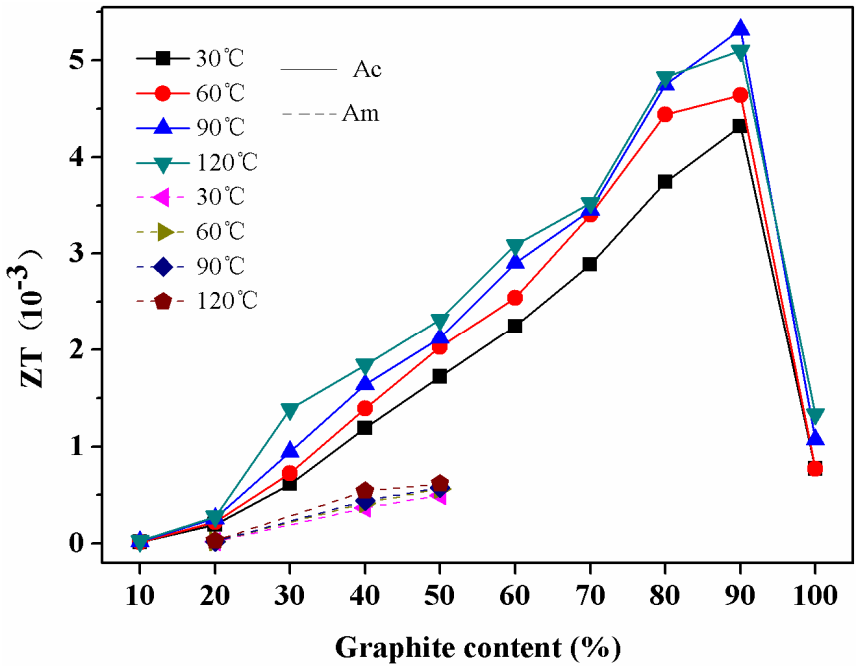

Fig. 13 ZT values of Am and Ac PMTDPABQ/G composites at different graphite contents

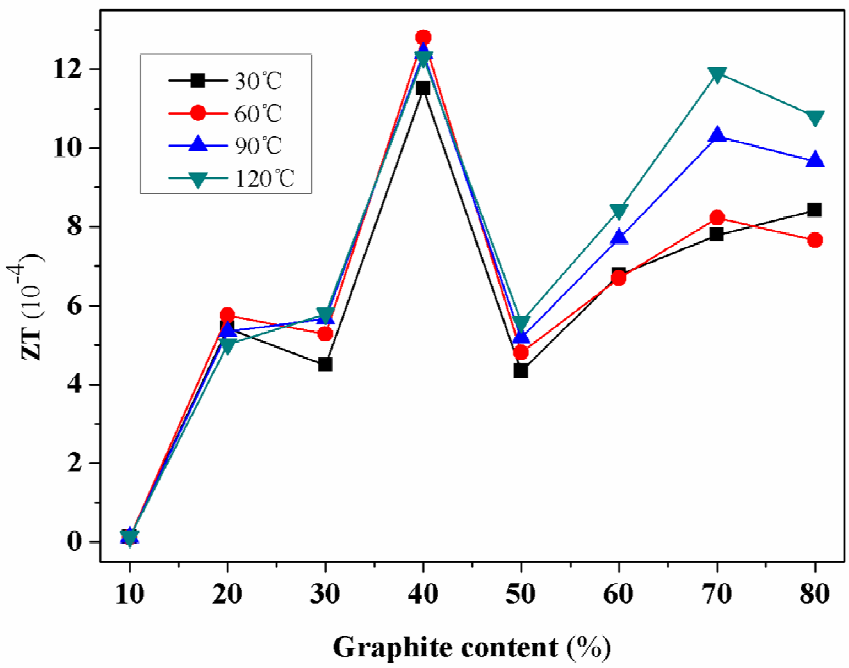

Fig. 14 ZT values of PTh/G composites at different graphite contents